Seventh Mississippi State - UAB Conference on Differential Equations and Computational Simulations, *Electronic Journal of Differential Equations*, Conf. 17 (2009), pp. 213–225.
ISSN: 1072-6691. URL: http://ejde.math.txstate.edu or http://ejde.math.unt.edu
ftp ejde.math.txstate.edu

OPTIMIZED DIFFERENCE SCHEMES FOR MULTIDIMENSIONAL HYPERBOLIC PARTIAL DIFFERENTIAL EQUATIONS

ADRIAN SESCU, ABDOLLAH A. AFJEH, RAY HIXON

Abstract. In numerical solutions to hyperbolic partial differential equations in multidimensions, in addition to dispersion and dissipation errors, there is a grid-related error (referred to as isotropy error or numerical anisotropy) that affects the directional dependence of the wave propagation. Difference schemes are mostly analyzed and optimized in one dimension, wherein the anisotropy correction may not be effective enough. In this work, optimized multidimensional difference schemes with arbitrary order of accuracy are designed to have improved isotropy compared to conventional schemes. The derivation is performed based on Taylor series expansion and Fourier analysis. The schemes are restricted to equally-spaced Cartesian grids, so the generalized curvilinear transformation method and Cartesian grid methods are good candidates.

1. Introduction

The numerical anisotropy is a type of error occurring in the numerical approximation of hyperbolic partial differential equations (PDE), using structured grids. This error can be reduced by using, for example, high-resolution difference schemes or sufficiently dense grids. While the former possibility requires special care at the boundaries, the latter might be computationally expensive. This work proposes a way to derive difference schemes in multidimensions that use points from more than one direction: the result is a improved isotropy of the wave propagation.

The optimization of the centered spatial differencing schemes in terms of lowering the dispersion error especially for Computational Aeroacoustics, Large Eddy Simulations and Direct Numerical Simulations is an actual field of research. Among others, the works of Lele [7] and Tam and Webb [11] are considered good starting points; the former conducted optimizations of Padé schemes using Fourier analysis, and the latter used the so-called dispersion-relation-preserving (DRP) concept to derive explicit high-resolution finite difference stencils. Kim and Lee [6] performed an analytic optimization of the compact finite difference schemes. They showed that an analytic optimization produces the maximum spatial resolution characteristics of the compact finite difference approximation in the evaluation of the

2000 *Mathematics Subject Classification.* 76Q05, 65M06, 65M20, 65Q05.
Key words and phrases. Computational aeroacoustics; isotropy error; difference methods.

Published April 15, 2009.

spatial finite derivatives. Li [8] has proposed new wavenumber-extended high-order upwind-biased schemes up to 11th-order by means of Fourier analysis. He showed that both the upwind-biased scheme of order 2N - 1 and the corresponding centered differencing scheme of order 2N have the same dispersion characteristics. Mahesh [10] derived a family of compact finite difference schemes for the spatial derivatives in the Navier-Stokes equations based on Hermite interpolation. He simultaneously solved for the first and second derivatives, getting higher-order of accuracy and better spectral resolution. Hixon [3] derived prefactored high-order compact schemes which use three-point stencils and return up to eighth-order accuracy. His schemes combine the tridiagonal compact formulation with the optimized split derivative operators of an explicit MacCormack type scheme. The tridiagonal matrix inversion was avoided by using bidiagonal matrices for the forward and backward operators. The optimization of Hixon's [3] schemes in terms of dispersion error was performed by Ashcroft and Zhang [1] who used Fourier analysis to select the coefficients of the biased operators, such that the dispersion characteristics match those of the original centered compact scheme and their numerical wavenumbers have equal and opposite imaginary components.

All of the above optimizations were performed in one-dimensional space and they may suffer from the isotropy error in multidimensions. An extended analysis of the isotropy error was performed by Vichnevetsky [14] who also solved the two-dimensional wave equation using two different schemes for the Laplacian operator, and averaged the two solutions. Considerable improvement of the isotropy of wave propagation was obtained based on variation of the weighted average. The same idea was considered by Trefethen [13] who used the leap frog scheme to solve the wave equation in two dimensions. Zingg and Lomax [16] performed optimizations of finite difference schemes applied to regular triangular grids, that give six neighbor points for a given node. Tam and Webb [12] proposed an anisotropy correction for Helmholtz equation; they found the anisotropy correction factor applicable to all noise radiation problems, irrespective of the complexity of the noise sources. Lin and Sheu [9] used the idea of DRP of Tam and Webb [11] in two dimensions to optimize the first-order spatial derivative terms of a model equation that resembles the incompressible Navier-Stokes momentum equation. They approximated the derivative using the nine-point grid system, resulting in nine unknown coefficients. Eight of them were determined by employing Taylor series expansions, and the remaining one was determined by requiring that the two-dimensional numerical dispersion relation is the same as the exact dispersion relation.

In this paper, multidimensional optimized schemes are derived using the weighted averaging technique and the transformation matrix between two orthogonal bases. Because the optimized schemes are linear combinations of classical finite difference schemes, they have the same order of accuracy as the corresponding classical schemes. Using Fourier analysis, their advantage is revealed in terms of isotropy error: compared to classical schemes, they have improved isotropy.

The organization of the paper is as follow. In Sec. II, the definition of the isotropy error is presented. In Sec. III, the dispersion relation for hyperbolic systems is determined. In Sec. IV, the procedure of deriving the optimized schemes is presented. In Sec. V the isotropy corrected factor is determined, and in Sec. VI, results for a problem from the First Computational Aeroacoustics Workshop [2] are reported. Concluding remarks are given in Sec. VII and the Taylor series

expansions for the second and fourth order optimized schemes are written in the appendix.

2. Isotropy error

Wave propagation is an inherent feature of the solutions of hyperbolic partial differential equations. In multidimensional space most of the waves or wave packets are propagating in all directions with the same phase or group velocity, respectively. A type of error occurring in the numerical approximation of hyperbolic equations in multidimensions is the numerical anisotropy. In addition to being dependent upon frequency, the numerical phase or group velocity is also dependent upon direction. The easiest way to illustrate this is by considering the advection equation in two dimensions:

$$\frac{\partial u}{\partial t} = \mathbf{c}\nabla u; \tag{2.1}$$

$$u(\mathbf{r}, 0) = u_0(\mathbf{r}) \tag{2.2}$$

where $\mathbf{r} = (x, y)$ is the vector of spatial coordinates, $\mathbf{c} = c(\cos\alpha \sin\alpha)$ is the velocity vector (c is scalar), $\nabla = (\partial/\partial x \partial/\partial y)^T$ and $u(x, y, t)$ and $u_0(\mathbf{r})$ are scalar functions.

A simple semi-discretization of the equation (2.1) is obtained with Cartesian coordinates on a square grid,

$$\frac{du}{dt} = -\frac{c}{2h}\big[\cos\alpha(u_{i+1,j} - u_{i-1,j}) + \sin\alpha(u_{i,j+1} - u_{i,j-1})\big] \tag{2.3}$$

where h is the grid step (the same in both directions). Consider the Fourier-Laplace transform:

$$\tilde{u}(k_1, k_2, \omega) = \frac{1}{(2\pi)^3}\int_0^\infty \int\int_{-\infty}^\infty u(x, y, t)e^{-i(kx\cos\alpha + ky\sin\alpha - \omega t)}dxdydt \tag{2.4}$$

and its inverse

$$u(x, y, t) = \int_\Gamma \int\int_{-\infty}^\infty \tilde{u}(k_1, k_2, \omega)e^{i(kx\cos\alpha + ky\sin\alpha - \omega t)}dk_1dk_2d\omega, \tag{2.5}$$

where $k\cos\alpha$ and $k\sin\alpha$ are the components of the wave number and ω is the frequency. Γ is a line parallel to the real axis in the complex ω-plane above all poles and singularities of the integrand (Tam and Webb, [11]). The application of Fourier-Laplace transform to Eq. (2.1) gives the exact dispersion relation:

$$\omega = ck(\cos^2\alpha + \sin^2\alpha) = ck \tag{2.6}$$

such that the phase velocity is obtained as

$$c_e = \frac{\omega}{k} = c \tag{2.7}$$

Plugging (2.6) back into (2.4), $u(x, y, t)$ is obtained as a superposition of sinusoidal solutions in the plane with constant phase lines given by

$$x\cos\alpha + y\sin\alpha - c_e t = \text{const.} \tag{2.8}$$

and, according to Eq. (2.7), the phase velocity, c_e, does not depend on direction (it is isotropic).

If the same is done for the numerical approximation, (2.2), the numerical dispersion relation takes the form:

$$\omega = \frac{c}{h}\big[\cos\alpha\sin(kh\cos\alpha) + \sin\alpha\sin(kh\cos\alpha)\big] \tag{2.9}$$

and the numerical phase velocity will be given by:

$$c_n = \frac{\omega}{k} = \frac{c}{kh}\big[\cos\alpha \sin(kh\cos\alpha) + \sin\alpha \sin(kh\cos\alpha)\big] \tag{2.10}$$

The constant phase lines are expressed by the equation

$$x\cos\alpha + y\sin\alpha - c_n t = const. \tag{2.11}$$

and moves with the phase velocity c_n. The numerical anisotropy is the effect of the numerical phase velocity which is dependent on direction.

The same considerations are valid for the group velocity defined as

$$g_e = \frac{\partial\omega}{\partial k} = c \tag{2.12}$$

showing that the exact group velocity is the same as the phase velocity because the dispersion relation is a linear function of k. But the numerical group velocity is different from the numerical phase velocity,

$$g_n = \frac{\partial\omega}{\partial k} = c\big[\cos^2\alpha\cos(kh\cos\alpha) + \sin^2\alpha\cos(kh\sin\alpha)\big], \tag{2.13}$$

which is also dependent on direction. This directional dependence (in both phase and group velocities) produces the numerical anisotropy.

3. Dispersion Relations for First Order Hyperbolic PDEs

Consider a hyperbolic set of first order partial differential equations defined in multidimensional space. Let Ω be an open subset in $\mathbf{R}^p$, and let $\mathbf{f}_j$, $1 \le j \le d$ be d smooth functions from Ω to $\mathbf{R}^p$. The general form is given by

$$\frac{\partial\mathbf{u}}{\partial t} + \sum_{j=1}^{d} \frac{\partial}{\partial x_j}\mathbf{f}_j(\mathbf{u}) = 0 \tag{3.1}$$

where

$$\mathbf{u} = (u_1 \dots u_p)^T \tag{3.2}$$

is a vector valued function and

$$\mathbf{f}_j = (f_{1j} \dots f_{pj})^T \tag{3.3}$$

is called flux vector. To simplify the analysis, suppose that the flux vector is a linear function of $\mathbf{u}$. Equation (3.1) written in primitive form is:

$$\frac{\partial u_i}{\partial t} + \sum_{j=1}^{d}\Big[\frac{\partial f_{ij}(u_i)}{\partial u_k}\Big]\frac{\partial u_i}{\partial x_j} = 0, \quad 1 \le i,k \le p \tag{3.4}$$

where the Einstein summation convention is used. The set of equations (3.1) is said to be hyperbolic if the eigenvalues associated with the matrix

$$\mathbf{B}(\mathbf{u},\alpha) = \sum_{j=1}^{d}\alpha_j\Big[\frac{\partial f_{ij}(u_i)}{\partial u_k}\Big]_{1\le i,k\le p} \tag{3.5}$$

are all real and the associated eigenvectors are linearly independent. The hyperbolicity implies that the initial set of equations admits wave-form solutions. The Fourier-Laplace transform to Eq. (3.3) yields a matrix equation:

$$\mathbf{A}\hat{\mathbf{u}} = \tilde{\mathbf{G}} \tag{3.6}$$

where $\tilde{\mathbf{G}}$ may result from the initial conditions. The dispersion relations associated with different waves are determined by making the determinant of the matrix $\mathbf{A}$ zero. This occurs when any of its eigenvalues is zero. If $(\lambda_i)_{q<i\leq m}$ are the $m-q+1$ eigenvalues corresponding to a type of wave, then the dispersion relation associated with this wave is defined as

$$\prod_{i=q}^{m} \lambda_i = 0 \tag{3.7}$$

All properties associated with that wave are encoded in the dispersion relation [15], and the specific errors (numerical dispersion, dissipation or anisotropy) that result from a particular numerical approximation are most commonly analyzed by comparing the numerical dispersion relation with the exact dispersion relation.

Example. Consider waves in a two-dimensional uniform, isentropic, subsonic compressible fluid flow $(\bar{u}, 0)$ along the x direction. For small perturbations in the density and the velocity components we may linearize and nondimensionalize the Euler equations of gas-dynamics, so that we the Linearized Euler Equations (LEE) are obtained:

$$\frac{\partial \mathbf{Q}}{\partial t} + \frac{\partial \mathbf{E}}{\partial x} + \frac{\partial \mathbf{F}}{\partial y} = 0 \tag{3.8}$$

where

$$\mathbf{Q} = \begin{pmatrix} \rho' \\ u' \\ v' \\ p' \end{pmatrix}, \quad \mathbf{E} = \begin{pmatrix} M\rho' + u' \\ Mu' + p' \\ Mv' \\ Mp' + u' \end{pmatrix}, \quad \mathbf{F} = \begin{pmatrix} v' \\ 0 \\ p' \\ v' \end{pmatrix} \tag{3.9}$$

ρ', u', v' and p' are the perturbations of density, x-component velocity, y-component velocity and pressure, respectively. M is the Mach number corresponding to the mean velocity.

The application of the Fourier-Laplace transform to (3.8) will generate the matrix

$$\mathbf{A} = \begin{pmatrix} \omega - k_1 M & -k_1 & -k_2 & 0 \\ 0 & \omega - k_1 M & 0 & -k_1 \\ 0 & 0 & \omega - k_1 M & -k_2 \\ 0 & -k_1 & -k_2 & \omega - k_1 M \end{pmatrix} \tag{3.10}$$

where k_1 and k_2 are the components of the wave number and ω is the frequency. It is easy to show that the eigenvalues of matrix $\mathbf{A}$ are

$$\begin{aligned} \lambda_1 = \lambda_2 &= \omega - k_1 M \\ \lambda_3 &= (\omega - k_1 M) + \sqrt{k_1^2 + k_1} \\ \lambda_4 &= (\omega - k_1 M) - \sqrt{k_1^2 + k_1} \end{aligned} \tag{3.11}$$

The first and the second eigenvalues (λ_1 and λ_2) correspond to entropy and vorticity waves, respectively. The third and the fourth (λ_3 and λ_4) correspond to acoustic waves, and the dispersion relation is given by

$$\lambda_3 \lambda_4 = (\omega - k_1 M)^2 - (k_1^2 + k_2^2) = 0 \tag{3.12}$$

For a stationary mean flow ($M = 0$) the dispersion relation (3.12) becomes

$$\omega^2 - (k_1^2 + k_2^2) = 0 \tag{3.13}$$

4. The Derivation of the Optimized Schemes

An equally-spaced, two-dimensional Cartesian grid is considered with i index on the x-direction and j index on the y-direction; the grid step is denoted by h. This kind of grid is typical to generalized curvilinear transormation methods, wherein the physical domain is mapped into the computational domain. Two orthogonal bases are considered, one (xOy) related to Cartesian grid directions and the other $(x'Oy')$ positioned at 45° with respect to the first. The transformation matrix between these two orthogonal bases is used to derive the optimized schemes:

$$\begin{pmatrix} x' \\ y' \end{pmatrix} = \begin{pmatrix} \cos\alpha & \sin\alpha \\ -\sin\alpha & \cos\alpha \end{pmatrix} \begin{pmatrix} x \\ y \end{pmatrix}, \tag{4.1}$$

where α is the angle between x and x' axes (45° in this case). The relation between the derivatives of a function (x, y) based on (4.1) is given by:

$$\begin{pmatrix} \frac{\partial u}{\partial x} \\ \frac{\partial u}{\partial y} \end{pmatrix} = \begin{pmatrix} \cos\alpha & -\sin\alpha \\ \sin\alpha & \cos\alpha \end{pmatrix} \begin{pmatrix} \frac{\partial u}{\partial x'} \\ \frac{\partial u}{\partial y'} \end{pmatrix}. \tag{4.2}$$

The general forms of classical difference schemes for the x- and y- derivatives are written as:

$$\Big(\frac{\partial v}{\partial x}\Big)_{i,j} = \sum_{\nu=-M}^{\nu=M} a_\nu \mathbf{E}_x^\nu \cdot v_{i,j} \tag{4.3}$$

and

$$\Big(\frac{\partial v}{\partial y}\Big)_{i,j} = \sum_{\nu=-M}^{\nu=M} a_\nu \mathbf{E}_y^\nu \cdot v_{i,j} \tag{4.4}$$

where multidimensional space shift operators (see Vichnevetsky and Bowles [14] for one dimension) are used:

$$\mathbf{E}_x^\nu \cdot v_{i,j} = v_{i+\nu,j}; \quad \mathbf{E}_y^\nu \cdot v_{i,j} = v_{i,j+\nu}. \tag{4.5}$$

The a_n coefficients are given in Table 1 for several frequently used centered schemes. By using the transformation matrix and a weighted averaging we get the optimized schemes in the form:

$$\Big(\frac{\partial v}{\partial x}\Big)_{i,j} = \frac{1}{h(1+\beta)} \sum_{\nu=-M}^{\nu=M} a_\nu \Big(\mathbf{E}_x^\nu + \frac{\beta}{2}\mathbf{D}_x\Big) \cdot v_{i,j} \tag{4.6}$$

and

$$\Big(\frac{\partial v}{\partial y}\Big)_{i,j} = \frac{1}{h(1+\beta)} \sum_{\nu=-M}^{\nu=M} a_\nu \Big(\mathbf{E}_y^\nu + \frac{\beta}{2}\mathbf{D}_y\Big) \cdot v_{i,j} \tag{4.7}$$

where the operators $\mathbf{D}_x^\nu\cdot$ and $\mathbf{D}_y^\nu\cdot$ are defined as

$$\mathbf{D}_x^\nu\cdot = \big(\mathbf{E}_x^\nu\mathbf{E}_y^\nu + \mathbf{E}_x^{-\nu}\mathbf{E}_y^\nu\big)\cdot; \quad \mathbf{D}_y^\nu\cdot = \big(\mathbf{E}_x^\nu\mathbf{E}_y^\nu + \mathbf{E}_x^\nu\mathbf{E}_y^{-\nu}\big)\cdot \tag{4.8}$$

The parameter β is called isotropy corrector factor (ICF).

The application of the Fourier transform to the schemes gives the numerical wavenumbers

$$(k_1h)_c^* = \sum_{n=-N}^{M} a_n e^{nIk_1h}, \quad (k_2h)_c^* = \sum_{n=-N}^{M} a_n e^{nIk_2h}, \tag{4.9}$$

TABLE 1. Coefficients of various explicit centered finite difference schemes.

Central scheme	$a_1 = -a_{-1}$	$a_2 = -a_{-2}$	$a_3 = -a_{-3}$
2^{nd} order centered	1/2	0	0
4^{th} order centered	2/3	-1/12	0
6^{th} order centered	3/4	-3/20	1/60
4^{th} order DRP	0.7708824	-0.1667059	0.0208431

for classical schemes and

$$(k_1h)^*_{opt} = \frac{2}{(1+\beta)} \sum_{n=-N}^{M} a_n \Big\{ e^{nIk_1h} + \frac{\beta}{2} \big[e^{nI(k_1+k_2)h} + e^{nI(k_1-k_2)h} \big] \Big\}, \tag{4.10}$$

$$(k_2h)^*_{opt} = \frac{2}{(1+\beta)} \sum_{n=-N}^{M} a_n \Big\{ e^{nIk_2h} + \frac{\beta}{2} \big[e^{nI(k_1\Delta x+k_2\Delta y)h} - e^{nI(k_1-k_2)h} \big] \Big\}, \tag{4.11}$$

for the optimized schemes ($I = \sqrt{-1}$) .

According to (3.13), and assuming that the time integration is free of numerical dissipation and dispersion, the numerical dispersion relation corresponding to two-dimensional wave equation is:

$$\omega^2 - \big[{(k_1h)^*_{opt}}^2 + {(k_2h)^*_{opt}}^2 \big] = 0. \tag{4.12}$$

which will be used in determining ICF (next section).

5. ICF Calculation

ICF is found by minimizing the integrated error between the phase or group velocities on x and $x = y$ directions. Let's consider two curves in wavenumber-frequency space: one of them is the intersection between the numerical dispersion relation surface and $k_2 = 0$ plane, and the other is the intersection between the numerical dispersion relation surface and the $k_1 = k_2$ plane. These two curves are superposed in the (kh, ω) plane, where

$$kh = \big[(k_1h)^2 + (k_2h)^2 \big]^{1/2} \tag{5.1}$$

Suppose that the equations of the two curves in $(k\Delta x, \omega)$ plane are

$$\omega_1 = \omega_1(kh, \beta), \quad \omega_2 = \omega_2(kh, \beta). \tag{5.2}$$

The integrated error between the phase velocities is then calculated on a specified interval,

$$C(\beta) = \int_0^\eta \big| c_1(kh, \beta) - c_2(kh, \beta) \big|^2 d(kh), \tag{5.3}$$

where

$$c_1(kh, \beta) = \frac{\omega_1(kh, \beta)}{kh}, \quad c_2(kh, \beta) = \frac{\omega_2(kh, \beta)}{kh} \tag{5.4}$$

are the numerical phase velocities. The upper limit of the integration, η, is a real number between 0 and π, and depends on the type of the scheme being optimized. The optimization can be also performed using the integrated error between the numerical group velocities,

$$G(\beta) = \int_0^\eta \big| g_1(kh, \beta) - g_2(kh, \beta) \big|^2 d(kh) \tag{5.5}$$

where

$$g_1(kh,\beta)=\frac{\partial\omega_1(kh,\beta)}{\partial(kh)},\quad g_2(k\Delta x,\beta)=\frac{\partial\omega_2(k\Delta x,\beta)}{\partial(k\Delta x)} \tag{5.6}$$

are the group velocities.

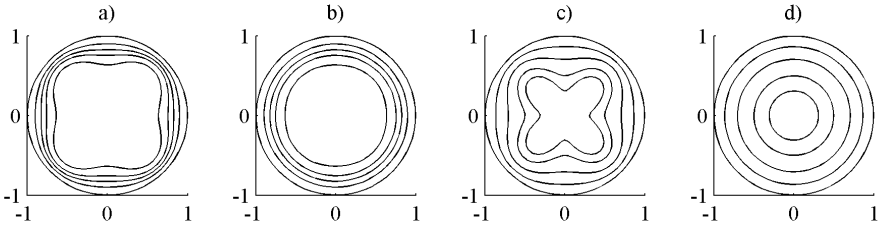

FIGURE 1. Polar diagram of normalized phase velocities (a and b) and group velocities (c and d) as a function of points per wavelength (PPW) and the direction of propagation: (a) and (c) using second-order classical schemes; (b) and (d) using second-order optimized schemes.

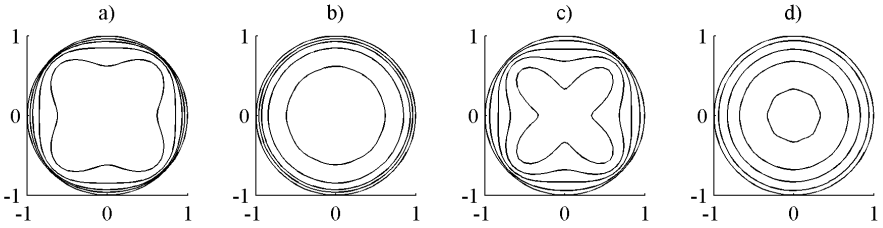

FIGURE 2. Polar diagram of normalized phase velocities (a and b) and group velocities (c and d) as a function of points per wavelength (PPW) and the direction of propagation: (a) and (c) using fourth-order classical schemes; (b) and (d) using fourth-order optimized schemes.

The minimization is done by equalizing the first derivative of $C(\beta)$ or $G(\beta)$ with zero:

$$\frac{dC(\beta)}{d\beta}=0\quad or\quad \frac{dG(\beta)}{d\beta}=0 \tag{5.7}$$

which gives the value of ICF, β . Corresponding to dispersion relation of the two-dimensional wave equation, for the second-order centered schemes $\beta\cong 0.53$, for the fourth-order centered schemes $\beta\cong 0.282$, and for the sixth-order centered schemes $\beta\cong 0.152$. In Figures 2 and 3 polar diagrams of normalized phase or group velocities for second and fourth order centered classical and optimized schemes are shown. The diagrams are plotted for different numbers of points per wavelength (PPW).

6. Numerical Tests

A two-dimensional problem from First Computational Aeroacoustics Workshop [2] is considered first. An acoustic wave initially situated in $O(0,0)$ point and an entropy wave in $P(67,67)$ point are convected with the mean flow along the $x=y$ direction. The linearized two-dimensional Euler equations are considered:

$$\frac{\partial \mathbf{Q}}{\partial t}+\frac{\partial \mathbf{E}}{\partial x}+\frac{\partial \mathbf{F}}{\partial y}=0 \tag{6.1}$$

where

$$\mathbf{Q}=\begin{pmatrix}\rho'\\ u'\\ v'\\ p'\end{pmatrix},\quad \mathbf{E}=\begin{pmatrix}M_x\rho'+u'\\ M_xu'+p'\\ M_xv'\\ M_xp'+u'\end{pmatrix},\quad \mathbf{F}=\begin{pmatrix}M_y\rho'+v'\\ M_yu'\\ M_yv'+p'\\ M_yp'+v'\end{pmatrix} \tag{6.2}$$

M_x and M_y are constant mean flow Mach number components in x and y directions, respectively. The computational domain embedded in free space is $-100<x<100$,$-100<y<100$, and x- and y-component of the Mach number are

$$M_x=M_y=0.5\cos\big(\frac{\pi}{4}\big) \tag{6.3}$$

The initial conditions are Gaussian impulses:

$$p'=e^{-(\ln 2)\left(\frac{x^2+y^2}{9}\right)}, \tag{6.4}$$

$$\rho'=e^{-(\ln 2)\left(\frac{x^2+y^2}{9}\right)}+0.1e^{-(\ln 2)\left(\frac{(x-67)^2+(y-67)^2}{25}\right)}, \tag{6.5}$$

$$u'=0.04(y-67)e^{-(\ln 2)\left(\frac{(x-67)^2+(y-67)^2}{25}\right)}, \tag{6.6}$$

$$v'=0.04(x-67)e^{-(\ln 2)\left(\frac{(x-67)^2+(y-67)^2}{25}\right)}. \tag{6.7}$$

The problem is solved using two types of optimized centered finite difference schemes (second and fourth order). The higher-order schemes (higher than fourth order) are not referred in this section, although the anisotropy optimization is acting properly. The domain was discretized using equally-spaced grid on x- and y-directions (table 2 summarizes the number of points of the grids). One and two rows of grid points were considered outside the boundary for the application of non-reflecting boundary conditions Tam and Webb [11, 12].

Table 2. Number of grid points used for different cases.

Schemes	Number of grid points
Second-order	400
Fourth-order	300

Filtering techniques with constant coefficients [5] were included to annihilate the spurious waves: sixth order filters are used. Low-Dissipation and -Dispersion 4-6 Runge-Kutta Scheme of Hu et. al [4] is used for time integration. Results for time equal to 80 are given in Figures 3 and 4. The numerical results are compared to analytical results.

In addition, some numerical tests on the stationary fluid ($Mx=My=0$) were conducted: acoustic wave is propagating from origin, and the entropy wave is neglected. The domain was extended to $-400<x<400$, $-400<y<400$, such

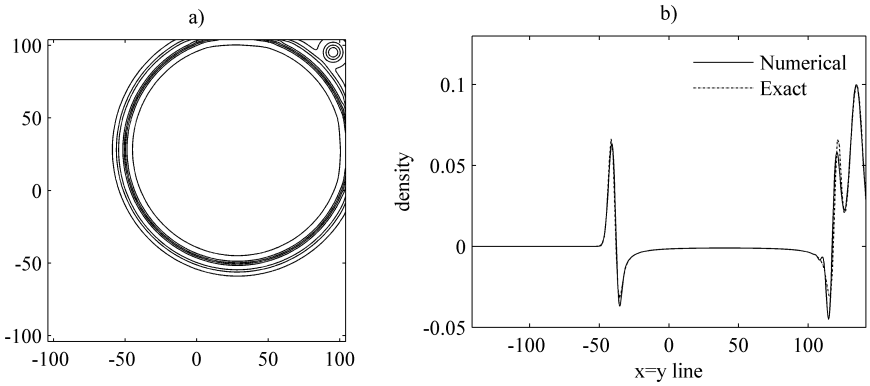

FIGURE 3. (a) Density contours and (b) density distribution along the x=y direction for the Computational Aeroacoustics Workshop problem using optimized second order schemes.

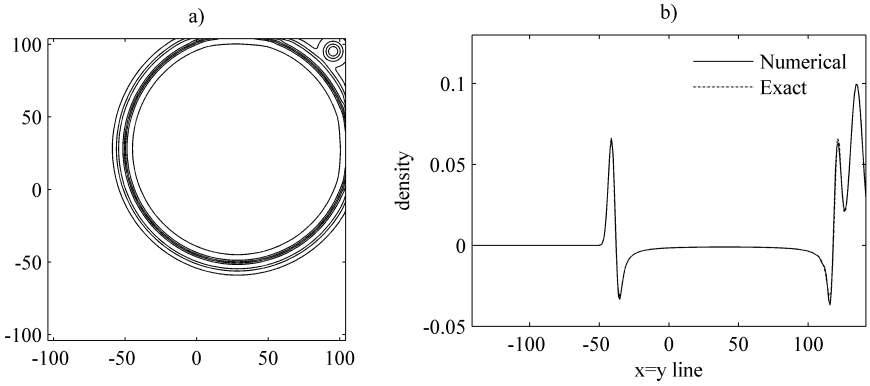

FIGURE 4. (a) Density contours and (b) density distribution along the $x = y$ direction for the Computational Aeroacoustics Workshop problem using optimized fourth order schemes.

that the wave can propagate for a longer distance. The front waves of the acoustic pressure on x, and $x = y$ directions are compared (Figure 5). The second order optimized centered schemes and their corresponding classical schemes are tested and compared this time in order to reveal the anisotropy correction. Figure 5(a) shows that the front waves computed using classical schemes do not coincide. In Figure 5(b) it is seen that the two front waves are matching by using optimized schemes.

Concluding Remarks. Anisotropy correction of multidimensional finite difference schemes was carried out for interior stencils. The optimized schemes incorporate a parameter called isotropy corrector factor (ICF) which can lower the isotropy error to a large extent. Based on Fourier analysis ICF was found and it was shown that, in terms of isotropy error, the optimized schemes are more effective compared to classical schemes. It was shown that the optimized schemes preserve the

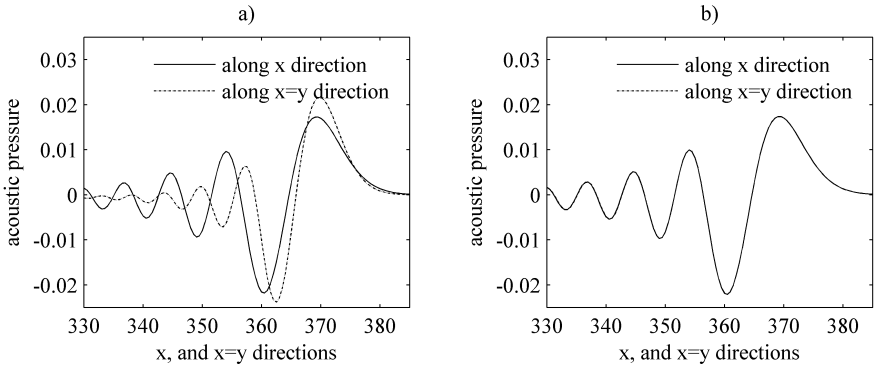

FIGURE 5. Superposed front waves on the x, and $x = y$ directions using (a) classical and (b) optimized second order schemes.

characteristics of the corresponding classical onedimensional schemes for all spatial directions. The optimized schemes are restricted to generalized curvilinear transformation and to Cartesian grid methods.

APPENDIX

In this appendix, it is shown that the order of accuracy of the second- and fourth-order optimized centered schemes is the same as that of the corresponding classical schemes. Only the coefficients in the Taylor series expansions and their summations are written. The grid is equally-spaced.

The coefficients of the Taylor series expansions for the second-order optimized scheme on the x direction are:

$$\frac{\partial^0 u}{\partial x^0}: \quad \frac{1}{2h(1+\beta)}\big[u_{i,j} - u_{i,j} + \frac{\beta}{2}(u_{i,j} - u_{i,j} + u_{i,j} - u_{i,j})\big], \tag{6.8}$$

$$\frac{\partial u}{\partial x}: \quad \frac{h}{2h(1+\beta)}\big[1 + 1 + \frac{\beta}{2}(1 + 1 + 1 + 1)\big] = \frac{2h(1+\beta)}{2h(1+\beta)} = 1, \tag{6.9}$$

$$\frac{\partial u}{\partial y}: \quad \frac{h}{2h(1+\beta)}\big[0 + \frac{\beta}{2}(1 - 1 - 1 + 1)\big] = 0, \tag{6.10}$$

$$\frac{\partial^2 u}{\partial x^2}: \quad \frac{h^2}{2h(1+\beta)}\big[\frac{1}{2!} - \frac{1}{2!} + \frac{\beta}{2}\frac{1}{2!}(1 - 1 + 1 - 1)\big] = 0, \tag{6.11}$$

$$\frac{\partial^2 u}{\partial x \partial y}: \quad \frac{h^2}{2h(1+\beta)}\big[0 + \frac{\beta}{2}\frac{1}{2!}(2 - 2 - 2 + 2)\big] = 0, \tag{6.12}$$

$$\frac{\partial^2 u}{\partial y^2}: \quad \frac{h^2}{2h(1+\beta)}\big[0 + \frac{\beta}{2}\frac{1}{2!}(1 - 1 + 1 - 1)\big] = 0. \tag{6.13}$$

The coefficients of the Taylor series expansions for the fourth-order optimized scheme on x direction are:

$$\frac{\partial^0 u}{\partial x^0}: \quad \frac{1}{12h(1+\beta)}\big[1 - 8 + 8 - 1 + \frac{\beta}{2}(1 - 8 + 8 - 1 + 1 - 8 + 8 - 1)\big] = 0, \tag{6.14}$$

$$\frac{\partial u}{\partial x}: \quad \frac{h}{12h(1+\beta)}\big[-2+8+8-2+\frac{\beta}{2}(-2+8+8-2-2+8+8-2)\big] = \frac{12h(1+\beta)}{12h(1+\beta)} = 1, \tag{6.15}$$

$$\frac{\partial u}{\partial y}: \quad \frac{h}{12h(1+\beta)}\big[0+\frac{\beta}{2}(-2+8+8-2+2-8-8+2)\big] = 0, \tag{6.16}$$

$$\frac{\partial^2 u}{\partial x^2}: \quad \frac{h^2}{12h(1+\beta)2!}\big[4-8+8-4+\frac{\beta}{2}(4-8+8-4+4-8+8-4)\big] = 0, \tag{6.17}$$

$$\frac{\partial^2 u}{\partial x \partial y}: \quad \frac{h^2}{12h(1+\beta)2!}\big[0+\frac{\beta}{2}(8-16+16-8+8-16+16-8)\big] = 0, \tag{6.18}$$

$$\frac{\partial^2 u}{\partial y^2}: \quad \frac{h^2}{12h(1+\beta)2!}\big[0+\frac{\beta}{2}(4-8+8-4+4-8+8-4)\big] = 0, \tag{6.19}$$

$$\frac{\partial^3 u}{\partial x^3}: \quad \frac{h^3}{12h(1+\beta)3!}\big[-8+8+8-8+\frac{\beta}{2}(-8+8+8-8-8+8+8-8)\big] = 0, \tag{6.20}$$

$$\frac{\partial^3 u}{\partial x^2 \partial y}: \quad \frac{h^3}{12h(1+\beta)3!}\big[0+\frac{\beta}{2}(-24+24+24-24+24-24-24+24)\big] = 0, \tag{6.21}$$

$$\frac{\partial^3 u}{\partial x \partial y^2}: \quad \frac{h^3}{12h(1+\beta)3!}\big[0+\frac{\beta}{2}(-24+24+24-24-24+24+24-24)\big] = 0, \tag{6.22}$$

$$\frac{\partial^3 u}{\partial y^3}: \quad \frac{h^3}{12h(1+\beta)3!}\big[0+\frac{\beta}{2}(-8+8+8-8+8-8-8+8)\big] = 0, \tag{6.23}$$

$$\frac{\partial^4 u}{\partial x^4}: \quad \frac{h^4}{12h(1+\beta)4!}\big[16-8+8-16+\frac{\beta}{2}(16-8+8-16+16-8+8-16)\big] = 0, \tag{6.24}$$

$$\frac{\partial^4 u}{\partial x^3 \partial y}: \quad \frac{h^4}{12h(1+\beta)4!}\big[0+\frac{\beta}{2}(64-32+32-64-64+32-32+64)\big] = 0, \tag{6.25}$$

$$\frac{\partial^4 u}{\partial x^2 \partial y^2}: \quad \frac{h^4}{12h(1+\beta)4!}\big[0+\frac{\beta}{2}(96-48+48-96+96-48+48-96)\big] = 0, \tag{6.26}$$

$$\frac{\partial^4 u}{\partial x \partial y^3}: \quad \frac{h^4}{12h(1+\beta)4!}\big[0+\frac{\beta}{2}(64-32+32-64-64+32-32+64)\big] = 0, \tag{6.27}$$

$$\frac{\partial^4 u}{\partial y^4}: \quad \frac{h^4}{12h(1+\beta)4!}\big[0+\frac{\beta}{2}(16-8+8-16+16-8+8-16)\big] = 0\,. \tag{6.28}$$

References

[1] G. Ashcroft and X. Zhang. Optimized prefactored compact schemes. *J. Comput. Phys.*, 190:459–477, 2003.

[2] J. C. Hardin, J. R. Ristorcelli, and C. K. W. Tam. ICASE/LaRC Workshop on Benchmark Problems in Computational Aeroacoustics (CAA). *NASA Conference Publication*, 3300, 1995.

[3] R. Hixon. Prefactored small-stencil compact schemes. *J. Comput. Phys.*, 165:522–541, 2000.
[4] F. Q. Hu, M. Y. Hussaini, and J. L. Manthey. Low-Dissipation and Dispersion Runge-Kutta Schemes for Computational Acoustics. *J. Comput. Phys.*, 124:177–191, 1996.
[5] C. A. Kennedy and M. H. Carpenter. Comparison of Several Numerical Methods for Simulation of Compressible Shear Layers. *Appl. Num. Math.*, 14:397–433, 1994.
[6] J. W. Kim and D. J. Lee. Optimized compact finite difference schemes with maximum resolution. *AIAA Journal*, 34 (5):887–893, 1996.
[7] S. K. Lele. Compact finite difference schemes with spectral-like resolution. *J. Comput. Phys.*, 103:16–42, 1992.
[8] Y. Li. Wave-Number Extended High-Order Upwind-Biased Finite-Difference Schemes for Convective Scalar Transport. *J. Comput. Phys.*, 133:235–255, 1997.
[9] R. K. Lin and Tony W. H. Sheu. Application of dispersion-relation-preserving theory to develop a two-dimensional convection-diffusion scheme. *J. Comput. Phys.*, 208:493, 2005.
[10] K. Mahesh. A family of high order finite difference schemes with good spectral resolution. *J. Comput. Phys.*, 145:332, 1998.
[11] C. K. W. Tam and J. C. Webb. Dispersion-Relation-Preserving Finite Difference Schemes for Computational Aeroacoustics. *J. Comput. Phys.*, 107:262–281, 1993.
[12] C. K. W. Tam and J. C. Webb. Radation Boundary Condition and Anisotropy Correction for Finite Difference Solutions of the Helmholtz Equation. *J. Comput. Phys.*, 113:122–133, 1994.
[13] L. N. Trefethen. Group Velocity in Finite Difference Schemes. *SIAM Rev.*, 24:113, 1982.
[14] R. Vichnevetsky and J. B. Bowles. *Fourier Analysis of Numerical Approximations of Hyperbolic Equations*. SIAM Studies in Applied Mathematics, Philadelphia, 1982.
[15] G. B. Whitham. *Linear and Nonlinear Waves*. A Wiley-Interscience Publication, New York, 1974.
[16] D. W. Zingg and H. Lomax. Finite Difference Schemes on Regular Triangular Grids. *J. Comput. Phys.*, 108:306–313, 1993.

Adrian Sescu
University of Toledo, Toledo, OH 43606, USA
E-mail address: asescu@utnet.utoledo.edu

Abdollah A. Afjeh
University of Toledo, Toledo, OH 43606, USA
E-mail address: aafjeh@utnet.utoledo.edu

Ray Hixon
University of Toledo, Toledo, OH 43606, USA
E-mail address: dhixon@utnet.utoledo.edu